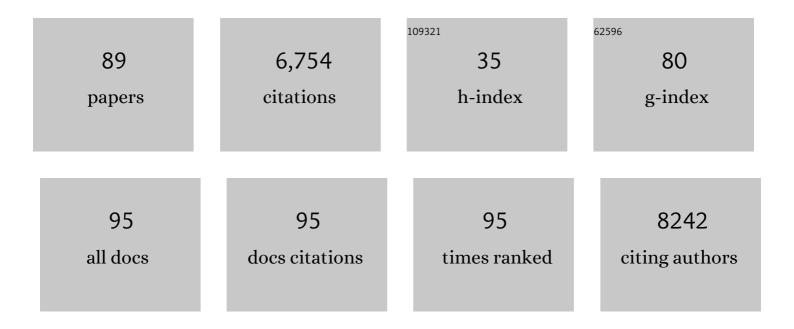
Hongbo Fu

List of Publications by Year in descending order

Source: https://exaly.com/author-pdf/259560/publications.pdf Version: 2024-02-01



HONGRO FU

#	Article	IF	CITATIONS
1	Visible-Light-Induced Degradation of Rhodamine B by Nanosized Bi2WO6. Journal of Physical Chemistry B, 2005, 109, 22432-22439.	2.6	1,170
2	A review of biomass burning: Emissions and impacts on air quality, health and climate in China. Science of the Total Environment, 2017, 579, 1000-1034.	8.0	815
3	Photocorrosion Inhibition and Enhancement of Photocatalytic Activity for ZnO via Hybridization with C ₆₀ . Environmental Science & Technology, 2008, 42, 8064-8069.	10.0	482
4	Photocatalytic Degradation of RhB by Fluorinated Bi ₂ WO ₆ and Distributions of the Intermediate Products. Environmental Science & Technology, 2008, 42, 2085-2091.	10.0	351
5	Photocatalytic properties of nanosized Bi2WO6 catalysts synthesized via a hydrothermal process. Applied Catalysis B: Environmental, 2006, 66, 100-110.	20.2	334
6	Synergetic Effect of Bi ₂ WO ₆ Photocatalyst with C ₆₀ and Enhanced Photoactivity under Visible Irradiation. Environmental Science & Technology, 2007, 41, 6234-6239.	10.0	326
7	Formation, features and controlling strategies of severe haze-fog pollutions in China. Science of the Total Environment, 2017, 578, 121-138.	8.0	245
8	Heterogeneous Uptake and Oxidation of SO2 on Iron Oxides. Journal of Physical Chemistry C, 2007, 111, 6077-6085.	3.1	202
9	Air pollution characteristics in China during 2015–2016: Spatiotemporal variations and key meteorological factors. Science of the Total Environment, 2019, 648, 902-915.	8.0	188
10	Electron Spin Resonance Spin-Trapping Detection of Radical Intermediates in N-Doped TiO2-Assisted Photodegradation of 4-Chlorophenol. Journal of Physical Chemistry B, 2006, 110, 3061-3065.	2.6	160
11	Synthesis, characterization and photocatalytic properties of nanosized Bi2WO6, PbWO4 and ZnWO4 catalysts. Materials Research Bulletin, 2007, 42, 696-706.	5.2	140
12	Spatial and temporal variation of particulate matter and gaseous pollutants in China during 2014–2016. Atmospheric Environment, 2017, 161, 235-246.	4.1	131
13	Photochemical formation of carbonate radical and its reaction with dissolved organic matters. Water Research, 2019, 161, 288-296.	11.3	86
14	Solubility of Iron from Combustion Source Particles in Acidic Media Linked to Iron Speciation. Environmental Science & Technology, 2012, 46, 11119-11127.	10.0	80
15	Photochemical Transformation of Aminoglycoside Antibiotics in Simulated Natural Waters. Environmental Science & Technology, 2016, 50, 2921-2930.	10.0	80
16	Identification of the typical metal particles among haze, fog, and clear episodes in the Beijing atmosphere. Science of the Total Environment, 2015, 511, 369-380.	8.0	69
17	Primary Particulate Matter Emitted from Heavy Fuel and Diesel Oil Combustion in a Typical Container Ship: Characteristics and Toxicity. Environmental Science & Technology, 2018, 52, 12943-12951.	10.0	69
18	Surface-Enhanced Raman Spectroscopy: A Facile and Rapid Method for the Chemical Component Study of Individual Atmospheric Aerosol. Environmental Science & Technology, 2017, 51, 6260-6267.	10.0	68

Номсво Fu

#	Article	IF	CITATIONS
19	Observation and analysis of atmospheric volatile organic compounds in a typical petrochemical area in Yangtze River Delta, China. Journal of Environmental Sciences, 2018, 71, 233-248.	6.1	66
20	Photoreductive dissolution of Fe ontaining mineral dust particles in acidic media. Journal of Geophysical Research, 2010, 115, .	3.3	65
21	Characteristics and chemical compositions of particulate matter collected at the selected metro stations of Shanghai, China. Science of the Total Environment, 2014, 496, 443-452.	8.0	64
22	Occurrence and estrogenic activity of steroid hormones in Chinese streams: A nationwide study based on a combination of chemical and biological tools. Environment International, 2018, 118, 1-8.	10.0	62
23	Characteristics of fine particle explosive growth events in Beijing, China: Seasonal variation, chemical evolution pattern and formation mechanism. Science of the Total Environment, 2019, 687, 1073-1086.	8.0	61
24	Development of Fluorescence Surrogates to Predict the Photochemical Transformation of Pharmaceuticals in Wastewater Effluents. Environmental Science & Technology, 2017, 51, 2738-2747.	10.0	58
25	An observational study of nitrous acid (HONO) in Shanghai, China: The aerosol impact on HONO formation during the haze episodes. Science of the Total Environment, 2018, 630, 1057-1070.	8.0	54
26	Satellite-based estimation of full-coverage ozone (O3) concentration and health effect assessment across Hainan Island. Journal of Cleaner Production, 2020, 244, 118773.	9.3	54
27	Observations of linear dependence between sulfate and nitrate in atmospheric particles. Journal of Geophysical Research D: Atmospheres, 2014, 119, 341-361.	3.3	45
28	Chemistry-triggered events of PM2.5 explosive growth during late autumn and winter in Shanghai, China. Environmental Pollution, 2019, 254, 112864.	7.5	44
29	Characterization of inorganic ions in rainwater in the megacity of Shanghai: Spatiotemporal variations and source apportionment. Atmospheric Research, 2019, 222, 12-24.	4.1	44
30	The contributions of socioeconomic indicators to global PM2.5 based on the hybrid method of spatial econometric model and geographical and temporal weighted regression. Science of the Total Environment, 2020, 703, 135481.	8.0	44
31	Satellite-based prediction of daily SO2 exposure across China using a high-quality random forest-spatiotemporal Kriging (RF-STK) model for health risk assessment. Atmospheric Environment, 2019, 208, 10-19.	4.1	42
32	The spatiotemporal variation and key factors of SO2 in 336 cities across China. Journal of Cleaner Production, 2019, 210, 602-611.	9.3	42
33	Long-range and regional transported size-resolved atmospheric aerosols during summertime in urban Shanghai. Science of the Total Environment, 2017, 583, 334-343.	8.0	41
34	Unexpectedly Increased Particle Emissions from the Steel Industry Determined by Wet/Semidry/Dry Flue Gas Desulfurization Technologies. Environmental Science & Technology, 2019, 53, 10361-10370.	10.0	39
35	Mechanistic Study of Visible-Light-Induced Photodegradation of 4-Chlorophenol by TiO _{2â~<i>x</i>} N <i>_x</i> with Low Nitrogen Concentration. International Journal of Photoenergy, 2012, 2012, 1-9.	2.5	38
36	Individual particle analysis of aerosols collected at Lhasa City in the Tibetan Plateau. Journal of Environmental Sciences, 2015, 29, 165-177.	6.1	38

Нолсво Fu

#	Article	IF	CITATIONS
37	Developing a novel hybrid model for the estimation of surface 8 h ozone (O ₃) across the remote Tibetan Plateau during 2005–2018. Atmospheric Chemistry and Physics, 2020, 20, 6159-6175.	4.9	35
38	The high-resolution estimation of sulfur dioxide (SO2) concentration, health effect and monetary costs in Beijing. Chemosphere, 2020, 241, 125031.	8.2	33
39	Trends in heterogeneous aqueous reaction in continuous haze episodes in suburban Shanghai: An in-depth case study. Science of the Total Environment, 2018, 634, 1192-1204.	8.0	32
40	Observations of atmospheric pollutants at Lhasa during 2014–2015: Pollution status and the influence of meteorological factors. Journal of Environmental Sciences, 2018, 63, 28-42.	6.1	31
41	Unique insights into photocatalytic VOCs oxidation over WO3/carbon dots nanohybrids assisted by water activation and electron transfer at interfaces. Journal of Hazardous Materials, 2022, 423, 127134.	12.4	31
42	Removal of SO ₂ on a nanoporous photoelectrode with simultaneous H ₂ production. Environmental Science: Nano, 2017, 4, 834-842.	4.3	30
43	Ligand-Promoted Photoreductive Dissolution of Goethite by Atmospheric Low-Molecular Dicarboxylates. Journal of Physical Chemistry A, 2017, 121, 1647-1656.	2.5	29
44	Atmospheric emissions of Cu and Zn from coal combustion in China: Spatio-temporal distribution, human health effects, and short-term prediction. Environmental Pollution, 2017, 229, 724-734.	7.5	28
45	Spatial and temporal variation of inorganic ions in rainwater in Sichuan province from 2011 to 2016. Environmental Pollution, 2019, 254, 112941.	7.5	28
46	Wet deposition of inorganic ions in 320 cities across China: spatio-temporal variation, source apportionment, and dominant factors. Atmospheric Chemistry and Physics, 2019, 19, 11043-11070.	4.9	28
47	Adsorption of SO2 on mineral dust particles influenced by atmospheric moisture. Atmospheric Environment, 2018, 191, 153-161.	4.1	26
48	Estimating historical SO2 level across the whole China during 1973–2014 using random forest model. Chemosphere, 2020, 247, 125839.	8.2	26
49	The variation of characteristics of individual particles during the haze evolution in the urban Shanghai atmosphere. Atmospheric Research, 2016, 181, 95-105.	4.1	25
50	Formation features of nitrous acid in the offshore area of the East China Sea. Science of the Total Environment, 2019, 682, 138-150.	8.0	25
51	Emerging investigator series: heterogeneous reactions of sulfur dioxide on mineral dust nanoparticles: from single component to mixed components. Environmental Science: Nano, 2018, 5, 1821-1833.	4.3	24
52	Real-time aerosol optical properties, morphology and mixing states under clear, haze and fog episodes in the summer of urban Beijing. Atmospheric Chemistry and Physics, 2017, 17, 5079-5093.	4.9	23
53	Substantial changes in gaseous pollutants and chemical compositions in fine particles in the North China Plain during the COVID-19 lockdown period: anthropogenic vs. meteorological influences. Atmospheric Chemistry and Physics, 2021, 21, 8677-8692.	4.9	22
54	Characterization of typical metal particles during haze episodes in Shanghai, China. Chemosphere, 2017, 181, 259-269.	8.2	20

Номсво Fu

#	Article	IF	CITATIONS
55	The effects of acetaldehyde, glyoxal and acetic acid on the heterogeneous reaction of nitrogen dioxide on gamma-alumina. Physical Chemistry Chemical Physics, 2016, 18, 9367-9376.	2.8	19
56	Enhanced heterogeneous uptake of sulfur dioxide on mineral particles through modification of iron speciation during simulated cloud processing. Atmospheric Chemistry and Physics, 2019, 19, 12569-12585.	4.9	18
57	Impact of adsorbed nitrate on the heterogeneous conversion of SO2 on α-Fe2O3 in the absence and presence of simulated solar irradiation. Science of the Total Environment, 2019, 649, 1393-1402.	8.0	17
58	The contributions of socioeconomic and natural factors to the acid deposition over China. Chemosphere, 2020, 253, 126491.	8.2	17
59	Characterization and acid-mobilization study for typical iron-bearing clay mineral. Journal of Environmental Sciences, 2018, 71, 222-232.	6.1	15
60	The influence of temperature on the heterogeneous uptake of SO2 on hematite particles. Science of the Total Environment, 2018, 644, 1493-1502.	8.0	15
61	A More Important Role for the Ozone (IV) Oxidation Pathway Due to Decreasing Acidity in Clouds. Journal of Geophysical Research D: Atmospheres, 2020, 125, e2020JD033220.	3.3	15
62	Estimating high-resolution PM1 concentration from Himawari-8 combining extreme gradient boosting-geographically and temporally weighted regression (XGBoost-GTWR). Atmospheric Environment, 2020, 229, 117434.	4.1	15
63	Effect of Formaldehyde on the Heterogeneous Reaction of Nitrogen Dioxide on Î ³ -Alumina. Journal of Physical Chemistry A, 2015, 119, 9317-9324.	2.5	14
64	Heterogeneous conversion of SO ₂ on nano α-Fe ₂ O ₃ : the effects of morphology, light illumination and relative humidity. Environmental Science: Nano, 2019, 6, 1838-1851.	4.3	14
65	Photochemical Oxidation of Water-Soluble Organic Carbon (WSOC) on Mineral Dust and Enhanced Organic Ammonium Formation. Environmental Science & Technology, 2020, 54, 15631-15642.	10.0	14
66	Physiochemical characteristics of aerosol particles collected from the Jokhang Temple indoors and the implication to human exposure. Environmental Pollution, 2018, 236, 992-1003.	7.5	13
67	Physiochemical characteristics of aerosol particles in the typical microenvironment of hospital in Shanghai, China. Science of the Total Environment, 2017, 580, 651-659.	8.0	11
68	Characteristics of the pollutant emissions in a tunnel of Shanghai on a weekday. Journal of Environmental Sciences, 2018, 71, 136-149.	6.1	11
69	Nitrous acid emission from open burning of major crop residues in mainland China. Atmospheric Environment, 2021, 244, 117950.	4.1	11
70	Phosphorus emission from open burning of major crop residues in China. Chemosphere, 2022, 288, 132568.	8.2	11
71	Spatiotemporal variation, source and secondary transformation potential of volatile organic compounds (VOCs) during the winter days in Shanghai, China. Atmospheric Environment, 2022, 286, 119203.	4.1	11
72	Effect of relative humidity and the presence of aerosol particles on the α-pinene ozonolysis. Journal of Environmental Sciences, 2018, 71, 99-107.	6.1	10

Номсво Fu

#	Article	IF	CITATIONS
73	The effects of surfactants on the heterogeneous uptake of sulfur dioxide on hematite. Atmospheric Environment, 2019, 213, 548-557.	4.1	10
74	A geographically and temporally weighted regression model for assessing intra-urban variability of volatile organic compounds (VOCs) in Yangpu district, Shanghai. Atmospheric Environment, 2019, 213, 746-756.	4.1	10
75	Chemical characterization and sources of PM2.5 at a high-alpine ecosystem in the Southeast Tibetan Plateau, China. Atmospheric Environment, 2020, 235, 117645.	4.1	10
76	Complexation of Fe(III)/Catechols in atmospheric aqueous phase and the consequent cytotoxicity assessment in human bronchial epithelial cells (BEAS-2B). Ecotoxicology and Environmental Safety, 2020, 202, 110898.	6.0	10
77	Long-term trends of ambient nitrate (NO ₃ ^{â^}) concentrations across China based on ensemble machine-learning models. Earth System Science Data, 2021, 13, 2147-2163.	9.9	10
78	The Sources and Atmospheric Pathway of Phosphorus to a High Alpine Forest in Eastern Tibetan Plateau, China. Journal of Geophysical Research D: Atmospheres, 2020, 125, e2019JD031327.	3.3	9
79	Estimation of relative water content in rice panicle based on hyperspectral vegetation indexes under water saving irrigation. Spectroscopy Letters, 2019, 52, 150-158.	1.0	8
80	Satellite-Based Estimates of Wet Ammonium (NH ₄ -N) Deposition Fluxes Across China during 2011–2016 Using a Space–Time Ensemble Model. Environmental Science & Technology, 2020, 54, 13419-13428.	10.0	8
81	Au nanoring arrays as surface enhanced Raman spectroscopy substrate for chemical component study of individual atmospheric aerosol particle. Journal of Environmental Sciences, 2021, 100, 11-17.	6.1	8
82	PM _{1.0} -Nitrite Heterogeneous Formation Demonstrated via a Modified Versatile Aerosol Concentration Enrichment System Coupled with Ion Chromatography. Environmental Science & Technology, 2021, 55, 9794-9804.	10.0	6
83	Preparation of nanosized Bi2WO6 using different content of starting materials and their photoactivities. Journal of Applied Spectroscopy, 2009, 76, 227-233.	0.7	4
84	Metals, PAHs and oxidative potential of size-segregated particulate matter and inhalational carcinogenic risk of cooking at a typical university canteen in Shanghai, China. Atmospheric Environment, 2022, 287, 119250.	4.1	4
85	Hyperspectral remote sensing to quantify the flowering phenology of winter wheat. Spectroscopy Letters, 2019, 52, 389-397.	1.0	3
86	Estimating monthly wet sulfur (S) deposition flux over China using an ensemble model of improved machine learning and geostatistical approach. Atmospheric Environment, 2019, 214, 116884.	4.1	3
87	Size-segregated water-soluble N-bearing species in the land-sea boundary zone of East China. Atmospheric Environment, 2019, 218, 116990.	4.1	2
88	High-resolution estimation of ambient sulfate concentration over Taiwan Island using a novel ensemble machine-learning model. Environmental Science and Pollution Research, 2021, 28, 26007-26017.	5.3	2
89	Size-Segregated Atmospheric Humic-Like Substances (HULIS) in Shanghai: Abundance, Seasonal Variation, and Source Identification. Atmosphere, 2021, 12, 526.	2.3	2